# Wideband operation of 3x3 Mach-Zehnder Interferometer mesh for programmable photonic computing

Wideband operation of 3x3 Mach-Zehnder Interferometer mesh for programmable photonic computing / Ma, T., Marchisio, A., Da Ros, F., Curri, V., Carena, A., Bardella, P.. - (2025). (2025 25th Anniversary International Conference on Transparent Optical Networks (ICTON) Barcellona (Spa) 6-10 Luglio 2025) [10.1109/ICTON67126.2025.11125174].

*Publisher:*
IEEE

*Published*
DOI:10.1109/ICTON67126.2025.11125174

# Wideband operation of 3x3 Mach-Zehnder Interferometer mesh for programmable photonic computing

Teng Ma
*Politecnico di Torino*
Torino, Italy
teng.ma@polito.it

Andrea Marchisio
*Politecnico di Torino*
Torino, Italy
andrea_marchisio@polito.it

Francesco Da Ros
*Technical University of Denmark*
Lyngby, Denmark
fdro@dtu.dk

Vittorio Curri
*Politecnico di Torino*
Torino, Italy
vittorio.curri@polito.it

Andrea Carena
*Politecnico di Torino*
Torino, Italy
andrea.carena@polito.it

Paolo Bardella
*Politecnico di Torino*
Torino, Italy
paolo.bardella@polito.it

***Abstract*—This work demonstrates the wideband performances of a 3-by-3 Mach-Zehnder Interferometer (MZI) mesh used as a programmable photonic logic gate. A digital twin of the device is created by fitting experimental data with a comprehensive circuit model that includes thermal effects. This model is used to identify voltage configurations to implement 15 user-defined Boolean functions at 1550 nm. These configurations are then tested across a large wavelength range (1524 nm – 1568 nm), which includes the entire C-band. Most test functions maintain correct operation across this range, with minor exceptions due to output connection issues. The results indicate a strong potential for wavelength division multiplexing (WDM) to perform multiple logic operations in parallel, boosting computational capabilities. The digital twin allows rapid testing and prototyping of photonic integrated circuits (PICs), supporting their use in photonic computing and AI hardware.**

***Index Terms*—Photonic computing, Mach-Zehnder Interferometers, Wideband operation.**

## I. INTRODUCTION

Artificial Intelligence (AI) and Machine Learning (ML) rely heavily on large amounts of data, which makes them very demanding in terms of computing power. To properly train a neural network (NN), the system needs to process millions of data samples. In fact, the computing power required for modern AI systems has been doubling roughly every 3.5 months [1]. However, improvements in traditional computer hardware have slowed down, especially due to the limits of Moore's law [2] and the inefficiency of the Von Neumann architecture in handling repeated mathematical operations like Multiply-Accumulate (MAC) [3]. As a result, there is a growing need for specialized hardware, called accelerators, that can handle these tasks more efficiently. One promising option is the use of Photonic Integrated Circuits (PICs) [4]. These can be built using networks of Mach-Zehnder Interferometers (MZIs), which perform the necessary linear calculations for NNs through thermal tuning. However, when these devices are packed closely together, problems such as heat interference between components (thermal crosstalk) [5] and manufacturing imperfections [6] strongly reduce the accuracy of the network unless properly managed.

In this work, we analyze the wideband properties of a device made up of 9 interconnected thermally-controlled MZIs, employed as a programmable photonic logic gate [7]. Using the analytical model for MZI-based meshed topologies first presented in [8], we demonstrate not only the ability of the reference photonic chip to implement user-defined Boolean logic functions, but also their robustness over a wide wavelength range. The capability of the reference chip to implement these Boolean functions on a wide band is especially promising because, on the one hand, it means that the implemented arbitrary functions are robust to wavelength fluctuations of the optical source; on the other hand, this feature also implies the possibility of performing multiple logic operations in parallel, leveraging the wideband reliability of the photonic circuit.

## II. REFERENCE DEVICE AND MODEL

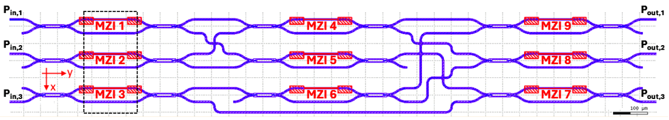

Fig. 1. Mask of the reference circuit. The waveguide structure is shown in blue, the Ti heaters in red. The black dashed rectangle indicates the area where our thermal analysis will be performed.

The device under test (Fig. 1) is a 3-by-3 mesh of interconnected MZIs, where the signals received at the three input ports are linearly combined at the three output through thermal tuning of the MZIs themselves. The single MZI is based on two 2-by-2 Multi-Mode Interferometers (MMIs) and ∼267 µm

---

A.M. Ph.D. scholarship is funded by the European Union Next-GenerationEU and by the Italian National Recovery and Resilience Plan (PNRR) through the Italian Ministry of University and Research (MUR) under grant D.M.352/2022.

979-8-3315-9777-1/25/$31.00 ©2025 IEEE

long bent waveguides, while the thermal tuning is regulated by a Thermo-Optic Phase Shifter (TOPS), implemented by a 100 µm Titanium strip on the upper branch of the interferometer. The device is a subsection of an optical switch for C-band operations, developed by the Technical University of Denmark (DTU) [9]. The PIC is designed on a silicon-on-insulator (SOI) platform with a top silicon thickness of 250 nm, with a buried aluminum mirror produced by flip bonding [9].

In order to simulate such a device, a transmission matrix-based model is used for the single device, first presented in [8]. Therefore, each section of the component (two MMIs and the propagation section) is described by a matrix that will be cascaded with the others to compute the output field.

$$\overline{T}_{\mathrm{MMI_{in}}} = \begin{bmatrix} \alpha_{\mathrm{MMI_{in}}}\sqrt{\gamma_1} & j\alpha_{\mathrm{MMI_{in}}}\sqrt{1-\gamma_2} \\ j\alpha_{\mathrm{MMI_{in}}}\sqrt{1-\gamma_1} & \alpha_{\mathrm{MMI_{in}}}\sqrt{\gamma_2} \end{bmatrix} \tag{1}$$

$$\overline{T}_{\mathrm{MMI_{out}}} = \begin{bmatrix} \alpha_{\mathrm{MMI_{out}}}\sqrt{\gamma_1} & j\alpha_{\mathrm{MMI_{out}}}\sqrt{1-\gamma_2} \\ j\alpha_{\mathrm{MMI_{out}}}\sqrt{1-\gamma_1} & \alpha_{\mathrm{MMI_{out}}}\sqrt{\gamma_2} \end{bmatrix} \tag{2}$$

$$\overline{T}_{\mathrm{p}} = \begin{bmatrix} e^{-\alpha_{\mathrm{p}}L}e^{j(\kappa n_{\mathrm{eff},1}(T)L+\delta\varphi)} & 0 \\ 0 & e^{-\alpha_{\mathrm{p}}L}e^{j(\kappa n_{\mathrm{eff},2}(T)L-\delta\varphi)} \end{bmatrix} \tag{3}$$

where $\alpha_{\mathrm{MMI}_k}$, $k = \{\text{in, out}\}$ are the insertion losses for input and output MMIs, $\gamma_i$ are the corresponding splitting ratios, $\alpha_{\mathrm{p}}$ are the propagation losses through the waveguide, $L$ is the length of the MZI arms, $\kappa = \frac{2\pi}{\lambda}$ is the wavenumber, with $\lambda$ wavelength of operation. The $\delta\varphi$ terms introduce a phase correction that can be fine-tuned with any optimization procedure (e.g., PSO [10]) in order to match experimental data accounting for fabrication variations.

Note that all the wavelength-dependent quantities ($\alpha_{\mathrm{MMI}}$, $n_{\mathrm{eff}}$, $\alpha_{\mathrm{p}}$, etc.) have been evaluated by means of Synopsys RSoft simulations to ensure an accurate wideband analysis.

Finally, the two quantities $n_{\mathrm{eff},1}(T)$ and $n_{\mathrm{eff},2}(T)$ represent the effective refractive indices of the two waveguides of the interferometer. The thermal dependence is due to the action of the TOPS: by applying a voltage on the Ti heater, the strip heats up due to the Joule heating effect and, consequently, the optical properties of the waveguide are modified. Note that the effective index $n_{\mathrm{eff}}$ of the two arms is different, since the effect of the heater will be more prevalent on the arm on which it is located. The dependency of $n_{\mathrm{eff}}$ on the temperature is expressed as a Taylor expansion:

$$n_{\mathrm{eff}}(T(V)) = n_{\mathrm{eff}}(T_0) + \left.\frac{\mathrm{d}n_{\mathrm{eff}}}{\mathrm{d}T}\right|_{T0}(T(V) - T_0) \tag{4}$$

In order to express the relationship between temperature $T$ and applied voltage $V$, instead of solving the heat diffusion problem, we decided to employ targeted COMSOL Multiphysics simulations, in which a single heater - waveguide system is simulated, to compute the spatial temperature distribution given an applied voltage. The spatial temperature distribution can be reconstructed for each vertical stack of MZIs by summing the three separate contributions at the correct applied voltage. The advantage of this approach is twofold: not only it allows us to avoid solving computationally intensive models for the Joule effect or performing time-consuming *ad hoc* COMSOL simulations, but it also allows us to automatically compute extended-scale effects, such as thermal crosstalk. Indeed, assuming that these effects have an impact only between MZIs on the same vertical column, with the presented method, we have the temperatures for each waveguide of each MZI at our disposal from the reconstructed spatial temperature distribution. Thanks to (4), these temperatures allow us to compute $n_{\mathrm{eff}}(T(V))$ in each waveguide; the refractive indices can then be used in (3), automatically taking into account the effect of the heating of each MZI on itself and on the neighboring components.

At this point, it is possible to compute the total transmission matrix by cascading the three constitutive elements of the MZI:

$$\overline{T} = \overline{T}_{\mathrm{MMI_{out}}}\overline{T}_{\mathrm{p}}\overline{T}_{\mathrm{MMI_{in}}} \tag{5}$$

This, of course, is employed to compute the output field at the two output ports of the MZI, given the amplitudes of the two input fields:

$$\begin{bmatrix} E_1^{\mathrm{out}} \\ E_2^{\mathrm{out}} \end{bmatrix} = \overline{T}\begin{bmatrix} E_1^{\mathrm{in}} \\ E_2^{\mathrm{in}} \end{bmatrix} \tag{6}$$

Applying a particle swarm optimization (PSO) [10], [11] to the previously described model, for each MZI of the mesh, we fine-tuned the parameter $\delta\varphi$ of Eq. (3) in order to obtain a more precise match of the trends resulting from the measurements of the reference circuit (Fig. 1). The advantage of this approach is twofold: not only this allows us to effectively account for the possible fabrication variations that may affect the operation of the real devices present in the mesh, but it also enables the creation of a full-fledged digital twin of the reference circuit that could be used for simulation purposes.

## III. WIDEBAND PROGRAMMABLE OPERATION

Using the calibrated model described in the previous section as a digital twin of the reference device, we explored the use of the reference MZI mesh as an arbitrary programmable logic gate by searching for the optimal driving conditions able to implement user-defined logic functions. The experimental evidence shows that the device exhibits wideband properties [12] and therefore the analysis is performed on the wavelength range from 1524 nm to 1568 nm.

Preliminarily, a complete analysis was performed at the nominal wavelength of 1550 nm [8]. Since the optical signals processed by means of the mesh are inherently analog, an intensity-based approach was adopted to perform the conversion to the digital domain: for each one of the three output ports, two separate thresholds are defined to discern logical 0s and 1s, based on the powers levels calculated at the output after the propagation through the device. Note that two different thresholds are used for each port, to create a gap separating the logical 0s and 1s, accounting for noise affecting the signals in a practical application; in this way

TABLE I

BOOLEAN FUNCTIONS EVALUATED BETWEEN 1524 NM AND 1568 NM. THE CASES MARKED WITH AN ASTERISK REQUIRE A CONSTANT INPUT SIGNAL $P_3 = 1$ TO IMPLEMENT THE DESIRED FUNCTION. X REPRESENTS DON'T-CARE; SP INDICATES "SUM OF PRODUCT" AND PS "PRODUCT OF SUM".

| Case | Description | $f_{\text{out},1}$ | $f_{\text{out},2}$ | $f_{\text{out},3}$ |
|---|---|---|---|---|
| 1 | No operation | $P_1$ | $P_2$ | $P_3$ |
| 2 | or/and | $P_1 + P_2 + P_3$ | X | $P_1 P_2 P_3$ |
| 3 | and/xor/or | $P_1 P_2$ | $P_1 \oplus P_2$ | $P_1 + P_2$ |
| 4 | and/and/xor | $P_1 P_2$ | $P_2 P_3$ | $P_1 \oplus P_3$ |
| 5 | or | $P_1 + P_2$ | $P_2 + P_3$ | $P_1 + P_3$ |
| 6* | nand/nor | X | $\overline{P_1 + P_2}$ | $\overline{P_1 P_2}$ |
| 7 | SP/PS | $(P_1 + P_2)P_3$ | $(P_1 P_2) + P_3$ | X |
| 8* | 2 bit not | $\overline{P_1}$ | X | $\overline{P_2}$ |
| 9 | Half adder | $P_1 \oplus P_2$ | X | $P_1 P_2$ |
| 10 | Full adder | $P_1 \oplus P_2$ | X | $P_2 P_3 + P_1(P_2 \oplus P_3)$ |
| 11 | Half subtractor | X | $P_1 \oplus P_2$ | $P_1 \overline{P_2}$ |
| 12 | 2bit 2's complement | $P_2 \oplus P_1 \oplus P_2$ | $P_1 \oplus P_2$ | X |
| 13 | 3bit 2's complement | $P_1$ | $P1 \oplus P_2$ | $(P_1 + P_2) \oplus P_3$ |
| 14 | Selectable and/or | $P_3(P_1 P_2) + \overline{P_3}(P_1 + P_2)$ | X | X |
| 15 | Selectable nor/or | $P_3(\overline{P_1 + P_2}) + \overline{P_3}(P_1 + P_2)$ | X | X |

the proposed methodology is more robust and independent of the input power. These thresholds are generated as follows. By randomizing the driving voltages $V_{\text{in}}$ of the 9 MZIs on the 0 V-2 V range and calculating output power for all $2^3$ possible combinations of input signals, a dataset with 6 million entries was created for each output port. Given these output power datasets, it is possible to define the thresholds:

$$S_{\text{d},k} = \begin{cases} 0, & P_{\text{a},k} \leq \kappa_0 \cdot P_{\text{m},k} \\ 1, & P_{\text{a},k} \geq \kappa_1 \cdot P_{\text{m},k} \end{cases} \tag{7}$$

where $S_{\text{d},k}$, with $k = \{1, 2, 3\}$, is the logical value resulting from the analog-to-digital conversion of the power measured at the $k$-th port, $P_{\text{a},k}$ is the power measured at the $k$-th port, and $P_{\text{m},k}$ is the median power value of the power distribution for the $k$-th output port. $\kappa_0 = 0.85$ and $\kappa_1 = 1.15$ are the weights used to distinguish the lower and upper thresholds. Any power value falling between these two values is discarded to prevent any issues related to power fluctuations.

After defining the thresholds for the analog-to-digital conversion, the optimal combination of 9 $V_{\text{in}}$ values to implement a user-defined truth table is searched using a PSO routine. The search starts from the data set entry that yields the best initial result and optimizes the distance between the output powers and the thresholds to enhance robustness. Multiple logic functions have been tested and are observed to match the target behavior (i.e. at least one driving voltage that reproduces the wanted truth table was found). A subset of the Boolean function combinations that were found to be working is listed in Tab. I, proving the capability of the device to implement diverse basic and complex user-defined logic functions.

In order to analyze the wideband capabilities of the reference device, the same procedure described previously is repeated for all 1 nm-spaced wavelengths in the range from 1524 nm to 1568 nm. This particular range is chosen as it is a subset of the range in which the experimental spectral response of the device is shown to be approximately flat [12]. Therefore, from 1524 nm to 1568 nm, with 1 nm step, a new data set is generated to define wavelength-specific thresholds.

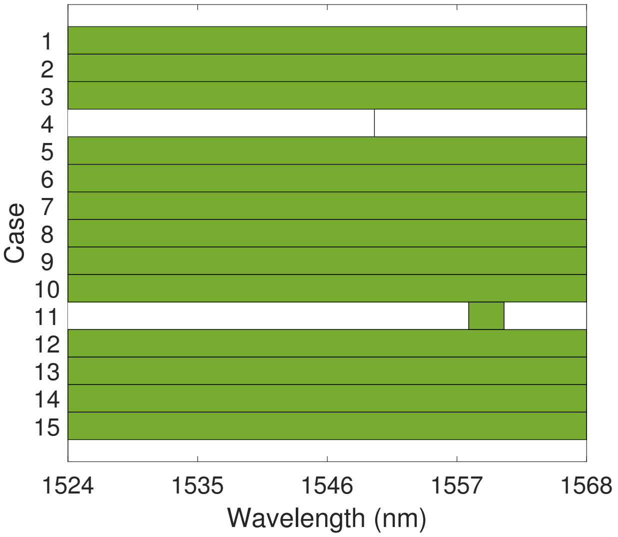

Fig. 2. Results of the wideband analysis. On the $x$ axis, the wavelength in nm; on the $y$ axis, the different user-defined Boolean functions of Tab. I. The largest continuous working bandwidth of each case is represented as a green bar.

Starting from the driving voltage combinations found at 1550 nm, we investigate how robust these results are in the 1524 nm–1568 nm range, i.e. whether the device, given the same 9 $V_{\text{in}}$ voltages, is capable to implement the same Boolean function at different wavelengths. For simplicity, we use the same thresholds for each wavelength that we consider, namely $P_{\text{m},k}$. In order to quantify the capability of the device to operate on multiple wavelengths, we introduce the following quantity, called "wideband robustness" $B_{\%}$, which represents a measure of the robustness of the $V_{\mathrm{in}}$ combination found at $\lambda = 1550\,\mathrm{nm}$ with respect to deviations from that nominal wavelength:

$$B_{\%} = \frac{\text{proper operation band}}{\text{considered band}} \times 100 \qquad (8)$$

When calculating this indicator, we consider a proper operation a situation in which the logical signals at the three output ports are all correct; separate $B_{\%}$ can be defined to describe the behavior of each port.

The results of the wideband analysis are reported in Fig. 2. The horizontal bars in this Figure represent the largest continuous working bandwidth for each Boolean function in Tab.I. The reported results confirm the expectations: the reference device shows wideband capabilities, and the programmed Boolean functions generally return the correct results on a large wavelength range. In fact, in 13 cases of the 15 reported in Tab. I the circuit is able to generate the desired truth table at all the ports in the entire wavelength range under test, corresponding to $B_{\%} = 100\%$.

Only two cases exhibit correct operation over a reduced bandwidth: case 4 (and/and/xor) shows a very selective behavior, returning the expected results only at the nominal 1550 nm, while for case 11 (half subtractor) the largest continuous interval for which the results are correct is 3 nm (from 1558 nm to 1561 nm), which corresponds to ($B_{\%} = 6.8\%$). In both cases, other single wavelengths work but are separate from the largest working range.

Moreover, in both cases 4 and 11, the results at ports 1 and 2 are correct on the whole wavelength range, while the limitation is due to port 3. Since there is no reason to expect a degradation of the accuracy of our model for port 3, we ascribe this phenomenon to the geometry of the device itself: indeed, as seen in Fig. 1, output port 3 is regulated by MZI 7, which receives one of the inputs directly from the first column of MZIs. This limited degree of optical processing could be the reason for the reduced robustness experienced in output 3.

Despite the presence of these two cases, Fig. 2 shows that the reference device simulated with our methodology holds promising resilience and robustness in the implementation of user-defined Boolean functions that are able to work on a large working bandwidth. Indeed, most of the tested functions can be reliably implemented on the whole C-band, opening the possibility of the implementation of parallelized logic operations by exploiting a WDM strategy.

## IV. CONCLUSIONS AND OUTLOOK

In this work, the wideband performance of a 3-by-3 Mach Zehnder Interferometer mesh used as a programmable photonic logic gate has been demonstrated. A digital twin of the device is obtained by fitting the experimental measurements with a comprehensive circuital model (including spurious thermal effects) and is used to find a combination of the nine driving voltages $V_{\mathrm{in}}$ that enables the implementation of user-defined Boolean functions at the nominal wavelength of 1550 nm. The voltages found to implement 15 different function combinations have then been tested in the wide wavelength range from 1524 nm to 1568 nm, which includes the entire C band.

The wideband analysis shows that most of the implemented functions yield the correct truth table on the entire wavelength range, with only two exceptions that could be mainly limited by the incomplete connections of output port 3. Despite these two cases, the other tested functions work on a wide range of wavelengths, which suggests the possibility of parallelizing multiple Boolean operations with a WDM strategy, strongly enhancing the computing power of this simple MZI-based meshed device.

These results highlight the promise of the proposed methodology: after a simple fitting of the measurements of the device, the user has a reliable digital twin of the real device at their disposal, which enables faster testing procedures that would be too time-consuming in a laboratory setting. Therefore, thanks to its fast simulations, such a tool can be a fundamental part of both testing existing PICs and prototyping new ones, in the context of AI accelerators or photonic computers.

## REFERENCES

[1] T. F. De Lima, H.-T. Peng, A. N. Tait, M. A. Nahmias, H. B. Miller, B. J. Shastri, and P. R. Prucnal, "Machine learning with neuromorphic photonics," *J. Lightwave Technol.*, vol. 37, no. 5, pp. 1515–1534, 2019.

[2] M. Waldrop, "More than Moore," *Nature News*, vol. 530, p. 144, 02 2016.

[3] H.-T. Peng, M. A. Nahmias, T. F. de Lima, A. N. Tait, and B. J. Shastri, "Neuromorphic photonic integrated circuits," *IEEE J. Sel. Top. Quantum Electron*, vol. 24, no. 6, pp. 1–15, 2018.

[4] L. De Marinis, M. Cococcioni, P. Castoldi, and N. Andriolli, "Photonic neural networks: A survey," *IEEE Access*, vol. 7, pp. 175827–175841, 2019.

[5] S. Biasi, R. Franchi, D. Bazzanella, and L. Pavesi, "On the effect of the thermal cross-talk in a photonic feed-forward neural network based on silicon microresonators," *Frontiers in Physics*, vol. 10, p. 1093191, 12 2022.

[6] M. Y.-S. Fang, S. Manipatruni, C. Wierzynski, A. Khosrowshahi, and M. R. DeWeese, "Design of optical neural networks with component imprecisions," *Opt. Express*, vol. 27, pp. 14009–14029, 05 2019.

[7] A. Marchisio, A. Cem, Y. Ding, V. Curri, A. Carena, F. Da Ros, and P. Bardella, "Optimization of 3x3 neuromorphic photonic network for programmable Boolean operations," in *SPIE Photonic West: Physics and Simulation of Optoelectronic Devices XXXII*, vol. 12880, pp. 191104–8, 2024.

[8] A. Marchisio, L. Tunesi, E. Ghillino, V. Curri, A. Carena, and P. Bardella, "Comprehensive thermal crosstalk model of meshed MZI topologies for neuromorphic computing," in *AI and Optical Data Sciences VI*, vol. 13375, p. 133750F, SPIE, 2025.

[9] Y. Ding, V. Kamchevska, K. Dalgaard, F. Ye, R. Asif, S. Gross, M. J. Withford, M. Galili, T. Morioka, and L. K. Oxenløwe, "Reconfigurable SDM switching using novel silicon photonic integrated circuit," *Scientific Reports*, vol. 6, no. 1, p. 39058, 2016.

[10] A. Marchisio, E. Ghillino, V. Curri, A. Carena, and P. Bardella, "Particle swarm optimization-assisted approach for the extraction of VCSEL model parameters," *Opt. Lett.*, vol. 49, pp. 125–128, 1 2024.

[11] J. Kennedy and R. Eberhart, "Particle swarm optimization," in *Proceedings of ICNN'95 - International Conference on Neural Networks*, vol. 4, pp. 1942–1948 vol.4, 1995.

[12] A. Cem, S. Yan, Y. Ding, D. Zibar, and F. Da Ros, "Data-driven modeling of mach-zehnder interferometer-based optical matrix multipliers," *J. Lightwave Technol.*, vol. 41, no. 16, pp. 5425–5436, 2023.